JOURNAL OF THERMOPHYSICS AND HEAT TRANSFER
Vol. 15, No. 3, July–September 2001

New Approach for Radiative-Transfer Computations in Axisymmetric Scattering Hot Media

Pierre-Emmanuel Baudoux,* Antoine Roblin,† and Patrick Chervet‡
ONERA, 91761 Palaiseau, France

An atmospheric three-dimensional discrete ordinate method, called the Spherical Harmonics Discrete Ordinate Method (SHDOM), is extended to nonequilibrium and axisymmetric media such as rocket plumes, which contain hot reactive gases and metallic oxide particles like alumina. A spherical harmonics base is used to improve the source function evaluation while solving the radiative-transfer equation. The source function includes the chemiluminescence radiation produced by gas reactions, the particles thermal radiation, and the in-scattering term. During the iteration process, the in-scattering term is evaluated with a spherical harmonics base using the radiance field calculated along discrete ordinates until the source function converges. Test cases in simple geometries, like plane parallel media or square enclosures, show the accuracy of SHDOM results according to others calculated by reference models. An extended Arrhenius law is used to model the middle-ultraviolet chemiluminescent radiation produced by the CO + O recombination. Finally, SHDOM is applied to the radiance field emitted by realistic rocket plume sections represented by infinite cylinders or finite cylindrical media shadowed by a mask representing the rocket body.

Nomenclature

A_λ	=	radial profile function for temperature and chemiluminescence
$A_\lambda^{\max}$	=	maximum of radial profile function A_λ
a	=	chemiluminescence volumetric power parameter
$B_\lambda(T)$	=	Planck function, W sr^{-1} m^{-2} μm^{-1}
b	=	thermal chemiluminescence volumetric power parameter, K
F^+	=	upper hemispherical flux
F^-	=	bottom "ground" hemispherical flux
$\tilde{F}^+$	=	net ground hemispherical flux
g	=	asymmetry parameter of the phase function
h	=	Planck constant, $6.626\,068\,76(52) \times 10^{-34}$ J s
I_λ	=	radiance, W sr^{-1} m^{-2} μm^{-1}
I_λ^C	=	chemiluminescent angular volumetric power, W sr^{-1} m^{-3} μm^{-1}
$I_{0,\lambda}^C$	=	chemiluminescent molar angular volumetric power, W sr^{-1} cm^3 mol^{-2} μm^{-1}
J_λ	=	emission source function, W sr^{-1} m^{-2} μm^{-1}
$\hat{J}_\lambda$	=	total source function, W sr^{-1} m^{-2} μm^{-1}
J_λ^S	=	in-scattering source function, W sr^{-1} m^{-2} μm^{-1}
L, M	=	spherical harmonic base truncation numbers
l, m	=	spherical harmonic order numbers
M	=	molecule or atom in the gas phase
N	=	number of discrete ordinates
N_μ	=	number of zenith angles
N_ϕ	=	maximum number of azimuthal angles
p_l	=	lth-order Legendre polynomial
R_0^C	=	chemiluminescent photon production rate, cm^3 mol^{-1} s^{-1}
R_σ	=	maximum radius of the cylinder containing particles, mm
$\boldsymbol{s}$	=	physical coordinate vector, m
T	=	temperature, K
X', X	=	x axis
Y', Y	=	y axis
Y_l^m	=	(l, m) spherical harmonics order
Z', Z	=	z axis
Θ	=	scattering angle
θ	=	zenithal angle
λ	=	wavelength, nm
ν	=	radiation frequency, Hz
σ	=	extinction coefficient, m^{-1}
τ	=	optical depth
Φ	=	scattering phase function, sr^{-1}
ϕ	=	azimuthal angle
χ_l	=	phase function Legendre coefficient
Ω	=	direction vector
ω_0	=	single scattering albedo

Received 23 March 2000; revision received 30 October 2000; accepted for publication 9 January 2001.

*Ph.D. Candidate, Département d'Optique Théorique et Appliquée, Chemin de la Hunière; baudoux@onera.fr.

†Research Engineer, Département d'Optique Théorique et Appliquée, Chemin de la Hunière; roblin@onera.fr.

‡Research Engineer, Département d'Optique Théorique et Appliquée, Chemin de la Hunière; chervet@onera.fr.

Introduction

RADIATIVE-TRANSFER modeling is needed in order to understand many physical problems such as heat transfer in furnaces or detectability of aircrafts and missiles. In most cases the optical signature of these flying objects, from infrared (IR) to UV comes from their motors' plume radiation.[1–3] The middle UV domain is of practical interest because the sky background seen from the low Earth atmosphere can be considered completely dark caused by solar radiation absorption by stratospheric and tropospheric ozone layers. This darkness allows one to detect a rocket plume with a good contrast, especially in the so-called solar blind band located approximately between 240 to 290 nm. The study of detection performance in this band requires data on UV plume signatures for various flight conditions and rocket motor types. As experimental results are limited to a few conditions, signature modeling is highly required to encompass all situations of practical interest. This modeling is performed in two steps. First the aerothermochemical plume properties are calculated using a suitable flowfield model,[4–6] and then the radiative-transferequation (RTE) is solved, based on calculated pressure, temperature, and species concentrations. The plumes are generally considered as axisymmetric media where emission, absorption, and scattering from metallic oxide (e.g., alumina) take place. Whereas molecular vibrational bands and thermal emission from particles are the principal sources in the IR, chemiluminescence reactions may become the dominant radiation mechanism in the UV.[1,3] In a rocket plume, reactions which result from a non-local

thermodynamic equilibrium coming from the combustion inside the plume, produce minor unstable species like atomic oxygen or the hydroxyl radical. Consequently, it is necessary to include the contribution of the chemiluminescent emission produced by these species in the source function. The purpose of this paper is to present a new radiative-transfer model adapted to UV plumes signature calculation, where particle scattering and a chemiluminescent gas are present.

The main difficulty in solving the RTE is the evaluation of the in-scattering contribution, which represents the radiation scattered by particles from all directions into the line of sight. Many methods, whose differences depend mainly upon the way in which scattering is considered, have been proposed over the last three decades for solving the RTE in scattering and participating media.[7] The zonal method[8] and the Monte Carlo[9] approach give accurate solutions, but computational time is so large that these techniques are restricted to simple geometric test cases and monochromatic or gray conditions. In the two-stream model,[10,11] where the radiance field is evaluated in two opposite propagation directions, the RTE is solved analytically in homogeneous media. However, this model provides only radiance estimations because of its poor angular resolution, and it is restricted to one-dimensional geometry. In the six-stream model,[12] which is the simplest three-dimensional model, the RTE is evaluated in three orthogonal directions. Yet the determination of radiance angular dependence requires as many computations as the number of the lines of sight required. The angular resolution provided by this model is still limited. In the discrete ordinate method (DOM) angular dependence is sampled in many directions defined by a quadrature scheme such as S_N (Ref. 13) or Gauss–Legendre.[14] Many authors have proposed ways to solve the DOM such as matrix inversion in plane parallel media[15] or iterative methods for three-dimensional problems.[16]

Evans[17] has developed an original extended iterative DOM for three-dimensional atmospheric problems called the Spherical Harmonics Discrete Ordinate Method (SHDOM). This model evaluates the in-scattering contribution using a spherical harmonics base, whereas the RTE is integrated along discrete ordinates defined in a Gauss–Legendre quadrature scheme. This artifice allows an interpolation of the radiance angular dependence, accelerates the computational process, and requires less computational time and memory storage. This code has been first applied to thermal problems in atmospheric media such as cloudy scenes and to scattering of IR-visible solar radiation. Because of its flexibility, the SHDOM approach has been found to be easily extended to nonequilibrium axisymmetric media such as rocket plumes. This paper will present such an extension in the UV domain. In the next section the main SHDOM features will be presented with the new developments needed in order to determine UV signature of rocket plumes. The reader is referred to Evans' original work[17] for details concerning SHDOM. Then, SHDOM results of simple validation test cases (plane parallel media and square enclosure) will be compared with results from other models published previously. After that the chemiluminescent reaction in the UV domain will be described. Finally, the modified SHDOM code will be applied to cylindrical media whose properties are similar to a realistic rocket plume.

Radiative Transfer Model

The monochromatic RTE describes the variation of the radiance field in a specified direction Ω through a small differential volume and can be written as

$$\frac{1}{\sigma(\boldsymbol{s},\lambda)}(\Omega\cdot\nabla)I_\lambda(\boldsymbol{s},\Omega) = -I_\lambda(\boldsymbol{s},\Omega) + J_\lambda(\boldsymbol{s},\Omega) + \frac{\omega_0(\boldsymbol{s},\lambda)}{4\pi}\int_{4\pi}\Phi(\boldsymbol{s};\lambda;\Omega'\to\Omega)I_\lambda(\boldsymbol{s},\Omega')\,\mathrm{d}\Omega' \tag{1}$$

where $I_\lambda(\boldsymbol{s},\Omega)$ is the radiance at point $\boldsymbol{s}$ propagating in direction Ω; $J_\lambda(\boldsymbol{s},\Omega)$ is the emission source function, which includes the particle thermal emission $[1-\omega_0(\boldsymbol{s},\lambda)]B_\lambda(T_{\text{Particles}})$ and chemiluminescence from gases $I_\lambda^C(\boldsymbol{s},\Omega)$ added in the modified model; $\sigma(\boldsymbol{s},\lambda)$ is the local extinction coefficient; $\omega_0(\boldsymbol{s},\lambda)$ is the single scattering albedo; and $\Phi(\boldsymbol{s};\lambda;\Omega'\to\Omega)$ is the normalized scattering phase function. The chemiluminescence $I_\lambda^C(\boldsymbol{s},\Omega)$ is introduced in the RTE as a volumetric angular power. So the emission source function should be written as

$$J_\lambda(\boldsymbol{s},\Omega) = [1-\omega_0(\boldsymbol{s},\lambda)]B_\lambda(T_{\text{Particles}}) + \frac{I_\lambda^C(\boldsymbol{s},\Omega)}{\sigma(\boldsymbol{s},\lambda)} \tag{2}$$

The in-scattering source function, which represents the radiation scattered by the particles from all directions into the direction of the line of sight, can be written as

$$J_\lambda^S(\boldsymbol{s},\Omega) = \frac{\omega_0(\boldsymbol{s},\lambda)}{4\pi}\int_{4\pi}\Phi(\boldsymbol{s};\lambda;\Omega'\to\Omega)I_\lambda(\boldsymbol{s},\Omega')\,\mathrm{d}\Omega' \tag{3}$$

The total source function $\hat{J}_\lambda(\boldsymbol{s},\Omega)$, which includes the emission term $J_\lambda(\boldsymbol{s},\Omega)$ and the in-scattering source function $J_\lambda^S(\boldsymbol{s},\Omega)$, is defined according to the following relation:

$$\hat{J}_\lambda(\boldsymbol{s},\Omega) = J_\lambda(\boldsymbol{s},\Omega) + J_\lambda^S(\boldsymbol{s},\Omega) \tag{4}$$

In the SHDOM approach, extended to the UV domain, the RTE is solved following these steps:

1) Initialization is where the RTE is integrated spatially column after column using a two-stream model (δ-Eddington).[18] The hemispherical fluxes are then converted to the first two moments of spherical harmonics of the radiance field.

2) The in-scattering source function $J_\lambda^S(\boldsymbol{s},\Omega)$ is evaluated with the spherical harmonics base using the radiance field calculated during the preceding step.

3) The total source function $\hat{J}_\lambda(\boldsymbol{s},\Omega)$, stored in the spherical harmonics base, is written in a discrete ordinates representation.

4) The RTE is integrated along each discrete ordinate with the total source function $\hat{J}_\lambda(\boldsymbol{s},\Omega)$ obtained during step 3, using a backward-ray scattering technique according to

$$I_\lambda(\boldsymbol{s},\Omega) = I_\lambda(0,\Omega)\exp\left[-\int_0^s\sigma(\boldsymbol{s}',\lambda)\,\mathrm{d}s'\right] + \int_0^s\exp\left[-\int_{s'}^s\sigma(\boldsymbol{s}'',\lambda)\,\mathrm{d}s''\right]\sigma(\boldsymbol{s}',\lambda)\hat{J}_\lambda(\boldsymbol{s}',\Omega)\,\mathrm{d}s' \tag{5}$$

5) The radiance field in discrete ordinates is converted to a spherical harmonic representation.

6) Steps 2–5 are continued until results converge according to a user-defined "solution criterion" based on an evaluation of the differences between current source function $\hat{J}_\lambda^{(n)}(\boldsymbol{s},\Omega)$ and the one calculated during the preceding iteration $\hat{J}_\lambda^{(n-1)}(\boldsymbol{s},\Omega)$.

7) The radiance field at a user-defined plane is extracted from the final source function field $\hat{J}_\lambda(\boldsymbol{s},\Omega)$ using the RTE integral form [Eq. (5)] as in step 4. The use of the spherical harmonics base allows the user to get the radiance field along other lines of sight than the SHDOM discrete ordinates.

The use of a real spherical harmonics base in SHDOM diagonalizes the phase function so that the in-scattering source function $J_\lambda^S(\boldsymbol{s},\Omega)$ can be written as

$$J_\lambda^S(\boldsymbol{s},\Omega) = \omega_0(\boldsymbol{s},\lambda)\sum_{l=0}^{L}\frac{\chi_l(\boldsymbol{s},\lambda)}{2l+1}\sum_{m=-M}^{M}I_{\lambda l}^m(\boldsymbol{s})Y_l^m(\Omega) \tag{6}$$

where (L, M) define the spherical harmonic base truncation, $I_{\lambda l}^m(\boldsymbol{s})$ is the (l,m)-order spherical harmonic coefficient of the radiance field, and $\chi_l(\boldsymbol{s},\lambda)$ the lth-order Legendre coefficient of the phase function defined by

$$\Phi(\boldsymbol{s};\lambda;\Omega'\to\Omega)\approx\sum_{l=0}^{L}\chi_l(\boldsymbol{s},\lambda)p_l(\cos\Theta) \tag{7}$$

The Gauss–Legendre quadrature scheme for discrete ordinates is defined by N_μ zenith angles with a maximum of N_ϕ azimuthal

angles (their number decreases as the zenith angle comes closer to the vertical direction). This user-defined setting determines the spherical harmonics truncation in accordance with

$$L = N_\mu - 1 \tag{8}$$

$$M = N_\phi/2 - 1 \tag{9}$$

This truncation preserves the spherical harmonics orthogonality in the angular quadrature scheme but may cause a misrepresentation of the particle scattering phase function leading to negative values. This situation is removed by applying the Delta-M method,[19] which renormalizes the phase function.

Because of the use of a spherical harmonic base, the iterations take less operations than a classical DOM. If N is the number of discrete ordinates, SHDOM takes, at each iteration, approximately N operations to evaluate the scattering integral and $9N^{3/2}$ others for conversions between the discrete ordinates and the spherical harmonic base. A classical DOM needs $2N^2$ operations for the same computation. SHDOM also needs less memory storage than a classical DOM. For example, with an angular resolution defined using N_μ zenith angles and $N_\phi = 2N_\mu$ azimuthal angles, a classical DOM stores the source function along $2N_\mu^2$ discrete ordinates. For the same angular resolution SHDOM reduces this number to N_μ^2 moments of spherical harmonics.

In the general case the medium's radiative properties are input in a property grid whose spatial structure is regular (even in X and Y, even or not in Z). During RTE integration [Eq. (5)], the extinction coefficient $\sigma(\boldsymbol{s}', \lambda)$ and its product with the total source function $\sigma(\boldsymbol{s}', \lambda)\hat{J}_\lambda(\boldsymbol{s}', \Omega)$ are assumed to be linear across every grid cell. If the total source function $\hat{J}_\lambda(\boldsymbol{s}', \Omega)$ is too heterogeneous and if the grid cell's optically thickness is higher than a user-defined splitting criterion, an adaptive grid algorithm is used to split the grid. The upper surface can be represented as a totally absorbing layer, which usually corresponds to the "sky" in atmospheric problems. In the same way the lower surface can be represented as a Lambertian "ground." The horizontal boundary conditions can be either "periodic" or "open." If boundary conditions are periodic, a ray exiting a vertical wall is continued on the opposite side as a new incident ray. Consequently the scene can be represented as an infinite mosaic whose period is given by the property grid size. In open boundary conditions radiative transfer is computed in two-dimensional mode on the vertical walls representing the infinite atmosphere surrounding the medium.

Computations on finite length axisymmetric media (e.g., rocket plumes) are performed with the vertical symmetric axis, and the vertical cell walls are transparent so that they do not affect the computational results with open boundary conditions. On the contrary, the symmetric axes of square enclosures or of infinite cylindrical media are horizontal in order to use the periodic boundary conditions. Because SHDOM has been initially developed in an atmospheric medium, it gives the radiance field only for a horizontal plane. Consequently, the code has been modified to allow radiance calculations in the vertical plane including the case where the line of sight is horizontal. In this way the radiance field cartography of a rocket plume can be rebuilt for any aspect angle. The plume intensity represents the whole radiative angular power received by a detector. It is calculated by surface integration of the radiance field, taking account of the perspective effect depending on the viewing angle.

Validation Test Cases

The aim of the validation test cases presented here is to compare the accuracy of SHDOM with other radiative-transfer models in well-known simple media. Two types of geometry are retained. Plane parallel media are used for comparison with the two-stream model, the six-stream model, and a reference DOM. These models have been used previously for rocket plume signatures.[12,20] Then, square enclosures are used to assess the SHDOM accuracy according to results from Liu et al.[21] More test cases have been performed by Evans[17] in order to establish the accuracy of SHDOM in various atmospheric problems (one-, two-, and three-dimensional). The author has concluded that SHDOM can be as accurate as a Monte–Carlo computation when the number of discrete ordinates is sufficiently large.

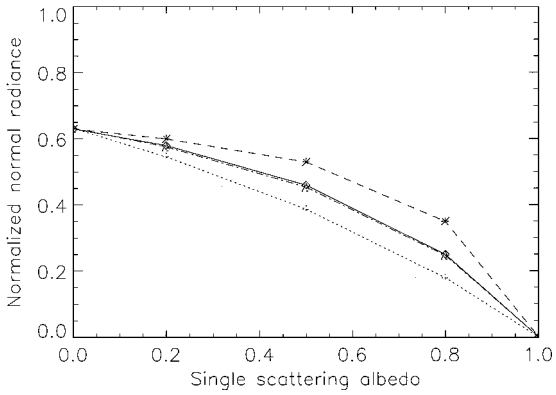

Fig. 1 Normal radiance $I_\lambda(z = Z; \theta = 0)/B_\lambda(T_0)$ vs single scattering albedo for a uniform plane parallel medium ($\tau = 1$, isotropic phase function) [+ · · · · +, two stream[12]; ∗– – –∗, six stream[12]; ◇——◇, N stream[12]; and △– – –△, SHDOM ($N_\mu = 20, N_\phi = 24$)].

Plane Parallel Medium

SHDOM calculations of the normal radiance exiting from thermally emitting plane parallel media have been compared with results obtained by Freeman et al.,[12] using the two- and six-stream models and a reference DOM, also called the N-stream model (with $N \gg 6$). The medium optical depth is equal to one. The SHDOM angular resolution is defined by $N_\mu = 20$ zenith angles and a maximum of $N_\phi = 24$ azimuthal angles. The property grid, defined by $5 \times 5 \times 6$ points, is a 1-m-per-side homogeneous cube. Because a plane parallel medium is infinite and homogeneous along the horizontal directions [$(X'X)$ and $(Y'Y)$], the boundary conditions are periodic in radiance through the vertical walls of the grid. Neither the ground nor the sky emit or reflect any radiation by themselves. The scattering phase function is assumed to be isotropic. The results are normalized by the radiance emitted by a Lambertian ground at the same temperature T_0 as the studied medium. Figure 1 shows the normal radiance $I_\lambda(z = Z; \theta = 0)/B_\lambda(T_0)$ calculated with the different methods vs the single scattering albedo. Although SHDOM gives the same results as the N-stream model, the two-stream and six-stream models respectively underpredict and overpredict radiance values. Freeman et al.[12] have shown that two-stream results are almost exact for a thin medium where lateral in-scattering can be neglected. Conversely, when the optical depth grows, the six-stream results are close to those of the N stream. In this situation the six-stream model evaluates correctly the lateral in-scattering effects. The test cases presented in Fig. 1 correspond to an intermediate situation where the two-stream and the six-stream approximations on the lateral in-scattering are both not adapted to evaluate the radiance field correctly.

Square Enclosure

The calculations presented next have been performed to establish the accuracy of SHDOM according to exact methods. As a discrete ordinate method, it can be used to compute hemispherical fluxes by radiance integration over $2\pi sr$. Comparing fluxes calculations with known exact results gives information on the correctness of the SHDOM radiance field angular representation used to evaluate the in-scattering source function $J_\lambda^S(\boldsymbol{s}, \Omega)$. Two test cases have been investigated: a thermally emitting and nonscattering two-dimensional medium in a square enclosure with 1-m-long sides, and a purely isotropically scattering medium illuminated by a nonreflecting thermally emitting Lambertian ground at temperature T_0. In both examples the cold and absorbing vertical boundaries, which are parallel to plane (YOZ), have been defined by optically thick and cold cells

Table 1 Number of discrete ordinates N and spherical harmonics N_{SH} used in SHDOM computations for the infinite square medium

Discrete ordinates			Spherical harmonics		
N_μ	N_ϕ	N (total number)	L	M	N_{SH} per point
2[a]	1	2	1	0	2
2[a]	4	8	1	1	4
8	16	90	7	7	64
16	32	354	15	15	256

[a] $\mu = \pm\sqrt{\frac{1}{3}}$.

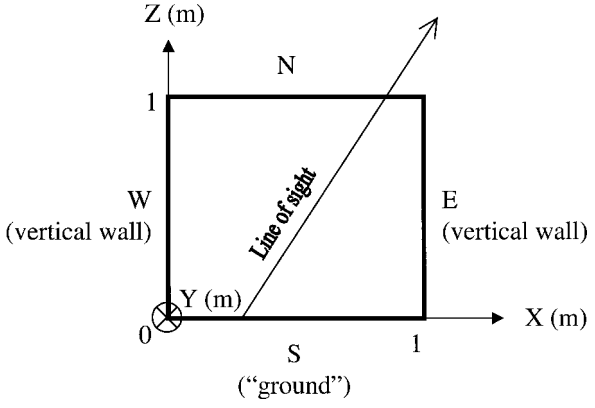

Fig. 2 Square enclosures geometry.

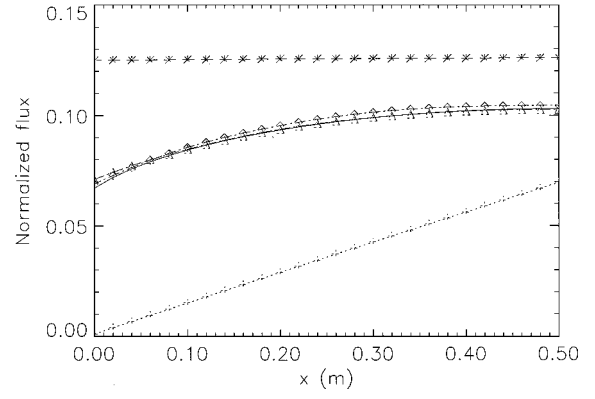

Fig. 3 Upper-wall hemispherical flux $F^+(x, z = Z)$ from a nonscattering and emissive infinite square enclosure with 1-m-long sides and an extinction coefficient σ equal to 0.1 m^{-1}: comparison between exact calculation and SHDOM computations with angular resolutions presented in Table 1 [——, exact calculation; + · · · · + , SHDOM ($N_\mu = 2, N_\phi = 1$); ∗- - -∗, ($N_\mu = 2, N_\phi = 4$); ◇- - -◇ ($N_\mu = 8, N_\phi = 16$); and △- - - -△, ($N_\mu = 16, N_\phi = 32$)].

(cf., Fig. 2). Radiance boundary conditions are periodic along direction $(Y'Y)$ so that the medium can be considered to be infinite in this direction. The elementary property grid length of the medium base is 0.02 m. Table 1 presents the angular resolution of SHDOM computations. The results are normalized by the hemispherical flux emitted by a Lambertian ground at the same temperature T_0 as the emitting component of the studied media. The temperature T_{cold} of the other items is set so that $B_\lambda(T_{cold}) \ll B_\lambda(T_0)$.

In the first test case the exact calculation has been performed by integrating exact radiance field over 100 zenith and 200 azimuthal angles. Figure 3 shows the normalized upper-hemispherical fluxes obtained from different angular resolutions in an optically thin

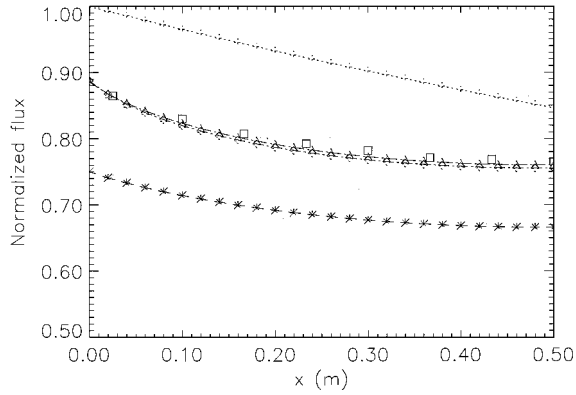

Fig. 4 Net ground hemispherical flux $\tilde{F}^+(x, z = 0)$ from a purely scattering infinite square enclosure with 1-m-long sides and an extinction coefficient σ equal to 1 m^{-1}: comparison between zone method and SHDOM computations with angular resolutions presented in Table 1 [□, zone method[21]; + · · · · + , SHDOM ($N_\mu = 2, N_\phi = 1$); ∗- - -∗, ($N_\mu = 2, N_\phi = 4$); ◇- - -◇ ($N_\mu = 8, N_\phi = 16$); and △- - - -△, ($N_\mu = 16, N_\phi = 32$)].

medium ($\sigma = 0.1\ m^{-1}$). The normalized upper-hemispherical fluxes are defined by

$$F^+(x, z = Z) = \frac{\displaystyle\int_0^{\pi/2} \cos\theta \sin\theta \, d\theta \int_0^{2\pi} I_\lambda(x, z = Z; \theta, \phi) \, d\phi}{\pi B_\lambda(T_0)} \tag{10}$$

Although results with $N_\mu = 2$ are obviously inaccurate, the computations converge to the exact solution with finer angular resolution. The resolution with ($N_\mu = 8$, $N_\phi = 16$) is suggested by Evans[17] to be optimal for flux calculations and with ($N_\mu = 16$, $N_\phi = 32$) for radiance computations. The pseudo two-stream and eight-stream schemes respectively under- and overpredict the horizontal direction contributions to the hemispherical fluxes. Because estimating the in-scattering source function [Eq. (3)] is similar to flux evaluation, these errors emphasize the difficulty to design an accurate two-stream model. In the second test case the exact results presented in Fig. 4 originating from Liu et al.[21] have been calculated using the zone method for $\sigma = 1\ m^{-1}$. The net ground hemispherical fluxes are defined by

$$\tilde{F}^+(x, z = 0) = 1 - F^-(x, z = 0) = 1 - \frac{\displaystyle\int_{\pi/2}^{\pi} \cos\theta \sin\theta \, d\theta \int_0^{2\pi} I_\lambda(x, z = 0; \theta, \phi) \, d\phi}{\pi B_\lambda(T_0)} \tag{11}$$

Although the two-stream and the eight-stream schemes respectively over- and underevaluate the in-scattering term, results with finer angular resolution are essentially coincident with the exact solution and the maximum differences are within 2%. Depending on the angular resolution and on the single scattering albedo, 1 to 10 iterations have been necessary to reach convergence.

CO + O Chemiluminescence

Combustion and afterburning processes in rocket plume produce molecular species such as CO_2, H_2O, CO, and reactive radicals like O and OH. The chemical reactions occurring between these molecules are able to produce a nonnegligible UV-visible photochemical emission, so-called chemiluminescence. In the solar blind spectral band the chemiluminescence comes mainly from the CO + O recombination,[3] which gives rise to a UV-visible continuum called CO blue flame emission:

$$CO + O \rightarrow CO_2 + h\nu \tag{12}$$

This reaction has been studied experimentally at low and high temperatures in many situations like flames,[22] shock waves,[23,24] or discharge tubes.[25] The principal properties of the CO + O radiative recombination mechanism are presented next. A semi-empirical law deduced from experimental reaction rates is then proposed.

The steps of the reactional mechanism depend on the electronic molecular states correlation[26] between these molecules as presented in Fig. 5. Pravilov and Smirnova[27] have proposed the following chemiluminescent mechanism:

$$CO(X^1\Sigma^+) + O(^3P) \leftrightarrow CO_2(^3B_2) \quad (13)$$

$$CO_2(^3B_2) \rightarrow CO_2(^1B_2) \quad (14)$$

$$CO_2(^1B_2) \rightarrow CO_2(X^1\Sigma_g^+) + h\nu \quad (15)$$

$$CO_2(^1B_2) + M \rightarrow CO_2(X^1\Sigma_g^+) + M \quad (16)$$

Spin conservation rules impose the restriction that the recombined $CO_2(^3B_2)$ is in a triplet state after reaction (13), which is the reverse of the $CO_2(^3B_2)$ predissociation. After a triplet-singlet transition [Eq. (14)] the de-excitation can be either radiative [Eq. (15)] or caused by collisions [Eq. (16)] with other molecules.

The experiment of Clyne and Trush[25] in discharge tubes at ambient temperature (293 K) and the study of Grillo and Slack[23] in hot shock waves (3000 K) show that chemiluminescent angular volumetric power I_λ^C is proportional to CO and O concentrations according to the following relation:

$$I_\lambda^C = I_{0,\lambda}^C[CO][O] \quad (17)$$

Slack and Grillo[28] have fit experimental results on chemiluminescent thermal dependence using an Arrhenius law, which can be expressed as photon production rate between 1300 K and 3000 K according to

Table 2 Experimental Arrhenius law parameters of CO + O chemiluminescence according to Eq. (17) whose results are given in units of W nm^{-1} sr^{-1} mol^{-2} cm^3

Wavelength, nm	$a(\lambda)$	$b(\lambda)$, K
255	17.67	4619
260	17.85	4582
280	18.67	4485
310	18.56	3039

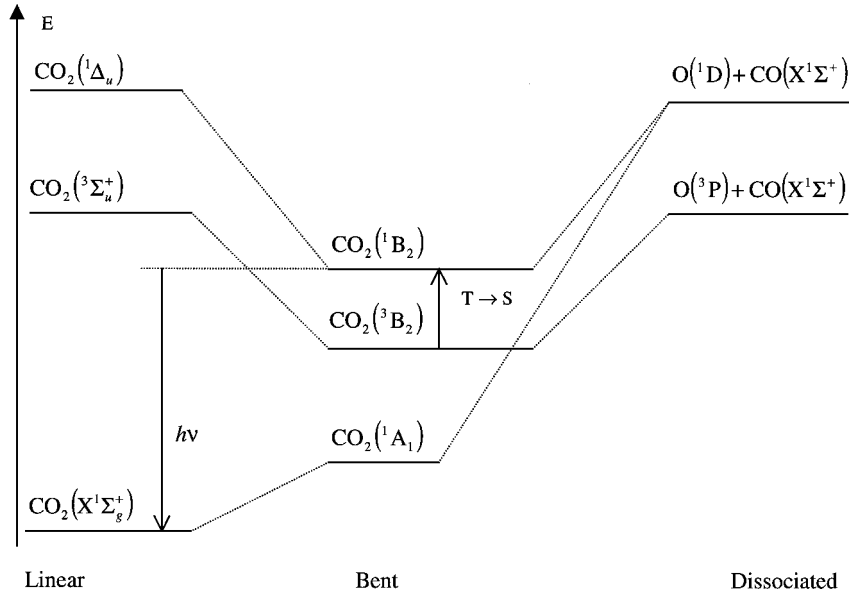

Fig. 5 Energy levels diagram of CO, O, and CO_2 (Ref. 26) (not to scale).

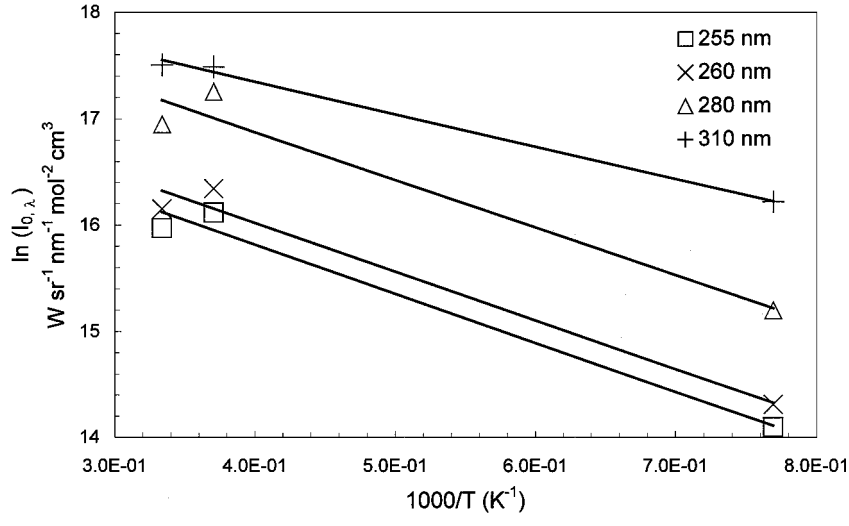

Fig. 6 Thermal dependence of the CO + O molar chemiluminescent volumetric angular power at several wavelengths in a logarithmic scale: experimental data from Grillo and Slack[23] (3000 K) and Slack and Grillo[28] (2700 and 1300 K).

$$R_0^C = 6.8(\pm 0.6) \times 10^5 \exp(-1960/T) \quad (18)$$

in units of $cm^3\ mol^{-1}\ s^{-1}$. The exponential coefficient 1960 K corresponds to the $CO_2(^3B_2)$ recombination [Eq. (11)] activation energy (about 0.17 eV). To describe the temperature dependence of the CO blue flame chemiluminescent spectrum, an extended Arrhenius law is used with wavelength-dependent coefficients:

$$I_{0,\lambda}^C = \exp[a(\lambda) - b(\lambda)/T] \quad (19)$$

where $I_{0,\lambda}^C$ is the chemiluminescent monochromatic volumetric angular power in units of $W\ nm^{-1}\ sr^{-1}\ mol^{-2}\ cm^3$. The parameters $a(\lambda)$ and $b(\lambda)$ (cf., Table 2) are deduced from the experimental Arrhenius diagram presented in Fig. 6.

UV Signature of Cylindrical Media

Radiance fields have been calculated with UV-extended SHDOM in simple cylindrical media. Four aerothermochemical profiles are deduced from flowfield calculations and are assumed to be independent of the axial coordinate. To simplify the presentation of the optical properties, their radial profiles, deduced from Mie theory and Eqs. (17) and (19), have been fitted with suitable functions. After a description of the radial profiles used, two test cases are presented corresponding to an infinite cylinder and a finite cylinder partially shaded by a mask.

Property Grid Settings

The extinction coefficient radial profile is assumed to be a straight line decreasing from the axis where $\sigma(0) = \sigma_{max}$ to the particle

Table 3 Settings of the cylinder test cases for the four media

Optical properties	Medium 1	Medium 2	Medium 3	Medium 4
Extinction coefficient, m^{-1}	Straight line	Straight line	Straight line	Straight line
	$\sigma_{max} = 15.0$	$\sigma_{max} = 12.5$	$\sigma_{max} = 7.5$	$\sigma_{max} = 4.5$
	$R_\sigma = 40$ mm	$R_\sigma = 60$ mm	$R_\sigma = 70$ mm	$R_\sigma = 100$ mm
Temperature, K	Double-Gaussian	Double-Gaussian	Gaussian	Gaussian
	$T_{max} = 2300$ K	$T_{max} = 2350$ K	$T_{max} = 2400$ K	$T_{max} = 2100$ K
	$T_0 = 2000$ K	$T_0 = 2200$ K	FWHM[a] = 35 mm	FWHM[a] = 40 mm
	$R_{max} = 15$ mm	$R_{max} = 10$ mm	——	——
Chemiluminescence, $W\ m^{-3}\ sr^{-1}\ \mu m^{-1}$	Double-Gaussian	Double-Gaussian	Double-Gaussian	Gaussian
	$C_{max} = 435.0$	$C_{max} = 395.0$	$C_{max} = 340.0$	$C_{max} = 65.0$
	$C_0 = 1.5$	$C_0 = 20.0$	$C_0 = 280.0$	FWHM[a] = 16 mm
	$R_{max} = 17$ mm	$R_{max} = 15$ mm	$R_{max} = 10$ mm	——

[a]Full width at half maximum.

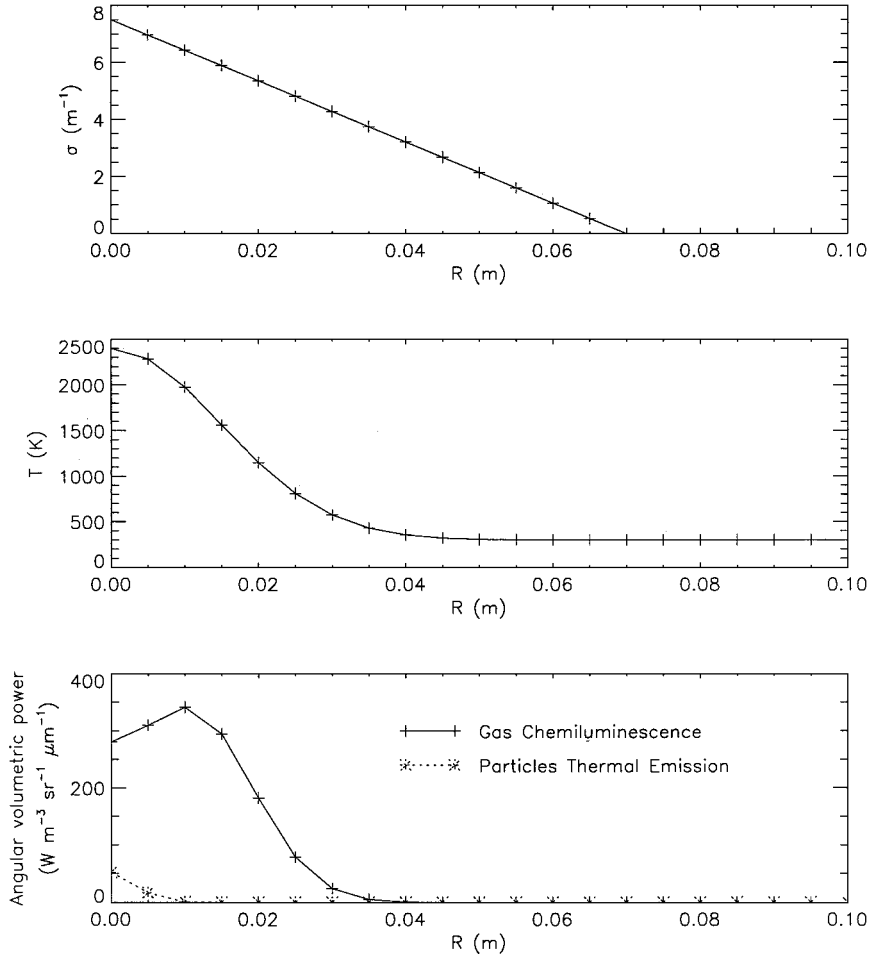

Fig. 7 Property radial profiles of cylindrical medium 3: particle extinction coefficient, temperature, and angular volumetric power from CO + O chemiluminescence and particle thermal emission.

radial extension R_σ. The minimum value of the extinction coefficient is equal to $\sigma_{\min} = 10^{-5}$ m^{-1} to avoid numerical artifacts during the source function $J_\lambda(s, \Omega)$ evaluation corresponding to chemiluminescence. The temperature axisymmetric profile and the chemiluminescence profile are defined either by a Gaussian curve or the sum of two Gaussian curves symmetric with the medium axis. They are parameterized by the axial value of the studied aerothermochemical property $A_\lambda(0)$, the maximum value $A_\lambda^{\max}$, and its radial position $R_{\max}$. The temperature curves have a lower limit $T_{\min} = 300$ K representing the atmospheric temperature. The RTE is solved in a rectangular parallelepipedic property grid. The radial extension (i.e., perpendicular to the medium axis) equals $2R_e = 200$ mm with a $\Delta r = 5$-mm elementary cell length. The angular resolution is defined with $N_\mu = 16$ zenith angles and a maximum of $N_\phi = 32$ azimuthal angles.

Table 3 summarizes the various parameters needed to describe the property profiles at 280 nm. Media 1 and 2 correspond to areas close to the nozzle, medium 3 corresponds to the afterburning zone (Fig. 7), and medium 4 represents the rocket plume tail. For a simple representation of the scattering properties, typical values have been used.[29] The single scattering albedo is uniformly equal to 0.8. To test our model, the phase function has been approximated as a Henyey–Greenstein phase function[30] with an asymmetry parameter g equal to 0.8.

Infinite Cylinder

Figure 8 represents the infinite cylinder geometry, and Fig. 9 shows the radiance profile of medium 3 for two aspect angles at 280 nm. Three iterations have been necessary to reach convergence. When the aspect angle decreases, the radiance values increase in the same manner as in the case of a thin emissive medium.[12] When integrated over a line of sight, the two peaks of medium 3's chemiluminescence radial profile disappear.

Rocket Body Masking

Figure 10 shows the geometry of the finite cylinder test case used to model the mask shadow's effect. The cylinder axis is vertical in order to use open boundary conditions. The cylinder is 1.04 m high with a spatial discretization equal to $\Delta z = 4$ mm. Figure 11 presents the intensity plot vs the aspect angle calculated with a mask radius equal to 40 mm. The intensity is deduced from the radiance field by a surface integration over one of the vertical walls and the upper horizontal plane. Media 1, 2, and 3 have intensity plots close to each other. Because medium 4 corresponds to the rocket plume tail, its intensity is small. The intensity's angular dependence can be explained by the extinction caused by the large particle concentration near the axis and, close to the nose-on aspect angle, by the mask shadow. The nose-on intensity is very small because the mask shades most of the chemiluminescent emission. Calculations with two mask radii presented in Table 4 also show that the nose-on intensity is very sensitive to the body masking size. Figure 12 shows the nose-on isoradiance curves for medium 3. The circular hole in the radiance field center corresponds to the mask, which hides a great part of the nose-on radiation. In this case the nose-on radiation depends largely on the mask size because it is on the same order as the plume radial extension. Other computations show that the nose-on intensity is lower in nonscattering cylindrical media than in the scattering cases. These results prove that scattering extends the apparent radial extension of rocket plumes at nose-on aspect.

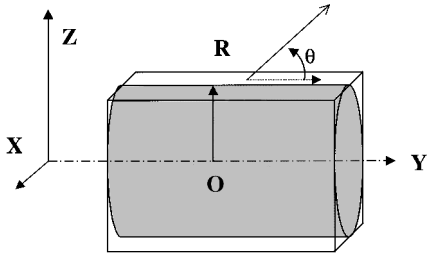

θ = aspect angle in plane (YOZ)

Fig. 8 Property grid geometry of infinite cylindrical media.

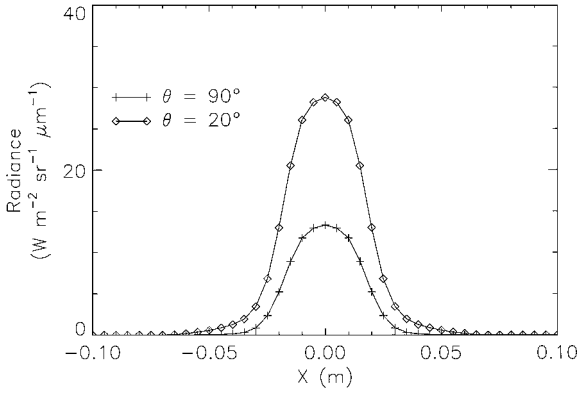

Fig. 9 Radiance profiles of medium 3 at 280 nm for two different aspect angles.

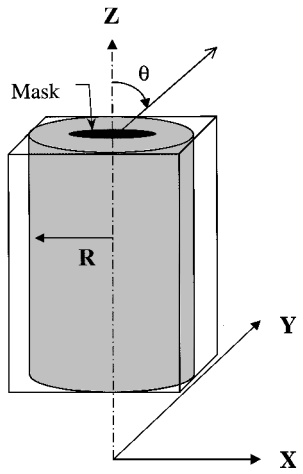

θ = aspect angle in plane (XOZ)

Fig. 10 Property grid geometry of the finite cylinder partially shaded by a circular mask.

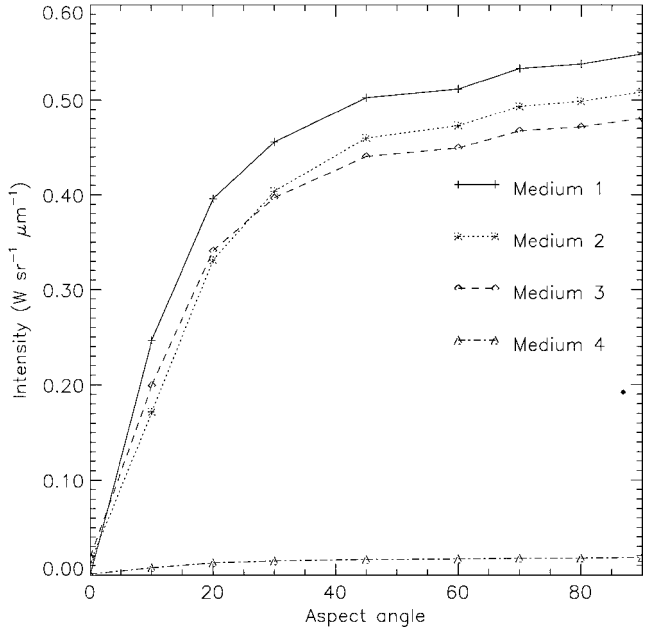

Fig. 11 Spectral intensity plot at 280 nm vs aspect angle for the different cylindrical media partially shaded by a circular mask, whose radius is equal to 40 mm.

Table 4 Nose-on intensity of the cylindrical media for several mask radii

R_{Mask}, mm	Nose-on intensity, mW sr^{-1} μm^{-1}			
	Medium 1	Medium 2	Medium 3	Medium 4
40	0.0	13.3	18.9	1.1
30	9.1	23.8	33.0	1.5

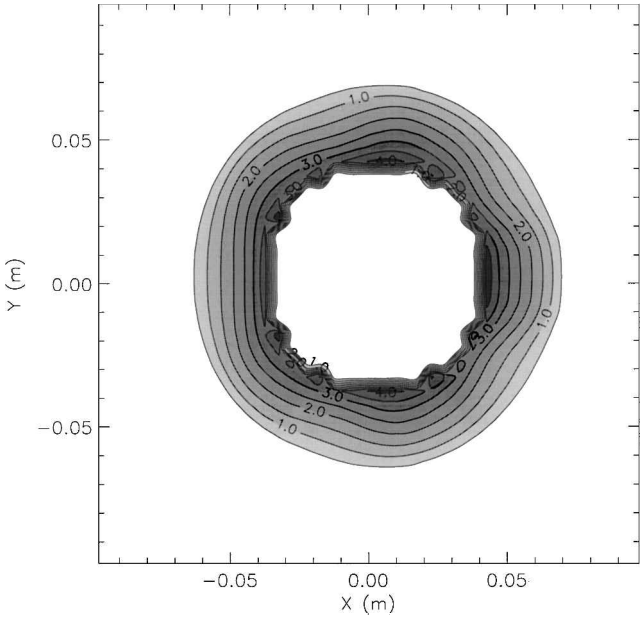

Fig. 12 Spectral nose-on radiance field at 280 nm (in W sr^{-1} m^{-2} μm^{-1}) of medium 3 partially shaded by a circular mask, whose radius is equal to 40 mm.

Conclusions

This paper has presented modifications of the atmospheric radiative transfer SHDOM applied to nonequilibrium media-like rocket plumes. The use of a spherical harmonics base in this DOM raises the in-scattering evaluation efficiency. This radiative field representation also allows radiance calculations along each user-defined line of sight. Test cases performed in simple geometries like plane parallel media or square enclosures show the accuracy of the SHDOM radiance and flux calculations and emphasize the lack of precision of radiative fields estimated by two- or six-stream models. UV CO + O chemiluminescence has been modeled with an extended Arrhenius law using experimental spectra. Finally, the improved SHDOM has been applied to cylindrical media defined using realistic plume section profiles. The infinite cylinder test case shows that the radiance field emitted by such media has an angular dependence similar to that of an optically thin medium for aspect angles close to a side-on view. The rocket body masking effects and the particle scattering role have been shown to be important for finite cylinder nose-on radiance fields. The results presented in this work attempt to demonstrate that the extended SHDOM is accurate, flexible, and easily applicable to a wide set of scattering media, in or out of thermal equilibrium, such as rocket plumes. As a three-dimensional radiative-transfer model, SHDOM is applicable to more realistic rocket plume modeling, in which the aerothermochemical properties depend on the distance from the nozzle. The use of SHDOM would carry out parametric studies on the influence of the optical properties of rocket plume's constituents upon its radiance field.

References

[1]Lyons, R. B., Wormhoudt, J., and Kolb, C. E., "Calculation of Visible Radiation from Missile Plumes," AIAA Paper 81-1111, June 1981.

[2]Lyons, R. B., Wormhoudt, J., and Gruninger, J., "Scattering Radiation in Low-Altitude Plumes," *Journal of Spacecraft and Rockets*, Vol. 20, No. 2, 1983, pp. 189–192.

[3]Kolb, C. E., Ryali, S. B., and Wormhoudt, J. C., "The Chemical Physics of Ultraviolet Rocket Plume Signature," *Ultraviolet Technology II*, SPIE Proceedings, Vol. 932, Society of Photo-Optical Instrumentation Engineers, Bellingham, WA, 1988, pp. 2–23.

[4]Dash, S. M., Pearce, B. E., Pergament, H. S., and Fishburne, E. S., "Prediction of Rocket Plume Flowfields for Infrared Signature Studies," *Journal of Spacecraft and Rockets*, Vol. 17, No. 3, 1980, pp. 190–199.

[5]Vitkin, E. I., Karelin, V. G., Kirllov, A. A., Suppurun, A. S., and Khadyka, J. V., "A Physico-Mathematical Model of Rocket Exhaust Plumes," *International Journal of Heat and Mass Transfer*, Vol. 40, No. 5, 1997, pp. 1227–1241.

[6]Rodionov, A. V., Plastinin, Y. A., Drakes, J. A., Simmons, M. A., and Hiers, R. S., "Modeling of Multiphase Alumina-Loaded Jet Flow Fields," AIAA Paper 98-3462, July 1998.

[7]Viskanta, R., and Mengüç, M. P., "Radiation Heat Transfer in Combustion Systems," *Progress in Energy Combustion Sciences*, Vol. 13, 1987, pp. 97–160.

[8]Bruyn, H. B., and Smith, T. F., "Development of the Zone Method for Linearly-Anisotropic Scattering Media," *Journal of Quantitative Spectroscopy and Radiative Transfer*, Vol. 40, No. 5, 1988, pp. 591–604.

[9]Lenoble, J., "Monte-Carlo Method," *Radiative Transfer in Scattering and Absorbing Atmospheres: Standard Computational Procedures*, A. Deepak Publishing, Hampton, VA, 1985, pp. 31–34.

[10]Meador, W. E., and Weaver, W. R., "Two-Stream Approximations to Radiative Transfer in Planetary Atmospheres: A Unified Description of Existing Methods and a New Improvement," *Journal of Atmospheric Sciences*, Vol. 37, No. 3, 1980, pp. 630–643.

[11]Toon, O. B., McKay, C. P., and Ackermann, T. P., "Rapid Calculation of Radiative Heating Rates and Photodissociation Rates in Inhomogeneous Multiple Scattering Atmospheres," *Journal of Geophysical Research*, Vol. 94, No. D13, 1989, pp. 16,287–16,301.

[12]Freeman, G. N., Ludwig, C. B., Malkmus, W., and Reed, R., "Development and Validation of Standardized Infrared Radiation Model (SIRRM) Gas/Particle Radiation Transfer Model," USAF/Air Force Rocket Propulsion Lab., AFRPL-TR-79-55, Edwards AFB, CA, Oct. 1979.

[13]Fiveland, W. A., "Discrete Ordinate Methods for Radiative Heat Transfer in Isotropically and Anisotropically Scattering Media," *Journal of Heat Transfer*, Vol. 109, 1987, pp. 809–812.

[14]Chandrasekar, S., "Quadrature Formulae," *Radiative Transfer*, Dover, New York, 1960, pp. 54–69.

[15]Stamnes, K., Tsay, S.-C., Wiscombe, W., and Jayaweera, K., "Numerically Stable Algorithm for Discrete-Ordinate-Method Radiative Transfer in Multiple Scattering and Emitting Layered Media," *Applied Optics*, Vol. 27, No. 12, 1988, pp. 2502–2509.

[16]Sanchez, A. A., Krajewsky, W. F., and Smith, T. F., "A General Radiative Transfer Model for Atmospheric Remote Sensing Studies in Multi-Dimensional Media," Iowa Inst. of Hydraulic Research, IIHR 355, Iowa City, IA, Jan. 1992.

[17]Evans, K. F., "The Spherical Harmonics Discrete Ordinate Method for Three-Dimensional Atmospheric Radiative Transfer," *Journal of Atmospheric Sciences*, Vol. 55, No. 3, 1998, pp. 429–446.

[18]Joseph, J. H., and Wiscombe, W. J., "The Delta-Eddington Approximation for Radiative Transfer," *Journal of Atmospheric Sciences*, Vol. 33, No. 12, 1976, pp. 2452–2459.

[19]Wiscombe, W. J., "The Delta-*M* Method : Rapid Yet Accurate Radiative Flux Calculations for Strongly Asymmetric Phase Function," *Journal of Atmospheric Sciences*, Vol. 34, No. 9, 1977, pp. 1408–1422.

[20]Ludwig, C. B., Malkmus, W., Freeman, G. N., Reed, R., and Slack, M., "Infrared Radiation from Rocket Plume," *Modern Utilization of Infrared Technology VI*, SPIE Proceedings, Vol. 253, Society of Photo-Optical Instrumentation Engineers, Bellingham, WA, 1980, pp. 122–128.

[21]Liu, J., Shang, H. M., Chen, Y. S., and Wang, T. S., "Analysis of Discrete Ordinates Method with Even Parity Formulation," *Journal of Thermophysics and Heat Transfer*, Vol. 11, No. 2, 1997, pp. 253–260.

[22]Samaniego, J.-M., Egolfopoulos, F. N., and Bowman, C. T., "CO_2^* Chemiluminescence in Premixed Flame," *Combustion Science and Technology*, Vol. 109, 1995, pp. 183–203.

[23]Grillo, A., and Slack, M., "CO + O Chemiluminescence: Rate Coefficient and Spectral Distribution," *Proceedings of the 13th International Symposium on Shock Tubes and Waves*, State Univ. of New York Press, Albany, NY, 1982, pp. 596–604.

[24]Eremin, A. V., and Ziborov, V. S., "Nonequilibrium Radiation from the CO_2 Band ($^1B_2 - X^l\Sigma_g^+$) in Shock-Heated Flows," *Shock Waves*, Vol. 3, 1993, pp. 11–17.

[25]Clyne, M. A. A., and Trush, B. A., "Mechanism of Chemiluminescent Combination Reactions Involving Oxygen Atoms," *Proceedings of the Royal Society of London*, Vol. 269A, 1962, pp. 404–418.

[26]Guidpati, M. S., "Photochemically Induced Electronic-to-Electronic Energy Transfer in Germinate $CO\cdots O$ van der Waals Pair Generated Through Vacuum Ultraviolet Photolysis of CO_2 in Ar Matrices," *Journal of Physical Chemistry A*, Vol. 101, No. 11, 1997, pp. 2003–2009.

[27]Pravilov, A. M., and Smirnova, L. G., "Temperature Dependence of the Spectral Distribution of the Rate Constant of Chemiluminescence in the Reaction $O(^3P) + CO \rightarrow CO_2 + h\nu$," *Kinetika i Kataliz*, Vol. 22, No. 4, 1981, pp. 832–838.

[28]Slack, M., and Grillo, A., "High Temperature Rate Coefficient Measurements of CO + O Chemiluminescence," *Combustion and Flame*, Vol. 59, 1985, pp. 189–196.

[29]Lyons, R. B., Wormhoudt, J., and Gruninger, J., "Scattering of Radiation by Particles in Low Atmospheric Plumes," AIAA Paper 81-1053, June 1981.

[30]Van de Hulst, H. C., "Results for the Henyey-Greenstein Phase Function, Unbounded and Semi-Infinite Medium," *Multiple Light Scattering Tables, Formula and Applications*, Vol. 2, Academic Press, New York, 1980, pp. 331–354.